

Grad-CL: Source Free Domain Adaptation with Gradient Guided Feature Disalignment

Rini Smita Thakur
rinitthakur@iiserb.ac.in

Rajeev Ranjan Dwivedi
rajeev22@iiserb.ac.in

Vinod K Kurmi
vinodkk@iiserb.ac.in

Department of Data Science and
Engineering
Indian Institute of Science Education
and Research Bhopal
India

Abstract

Accurate segmentation of the optic disc and cup is critical for the early diagnosis and management of ocular diseases such as glaucoma. However, segmentation models trained on one dataset often suffer significant performance degradation when applied to target data acquired under different imaging protocols or conditions. To address this challenge, we propose **Grad-CL**, a novel source-free domain adaptation framework that leverages a pre-trained source model and unlabeled target data to robustly adapt segmentation performance without requiring access to the original source data. Grad-CL combines a gradient-guided pseudolabel refinement module with a cosine similarity-based contrastive learning strategy. In the first stage, salient class-specific features are extracted via a gradient-based mechanism, enabling more accurate uncertainty quantification and robust prototype estimation for refining noisy pseudolabels. In the second stage, a contrastive loss based on cosine similarity is employed to explicitly enforce inter-class separability between the gradient-informed features of the optic cup and disc. Extensive experiments on challenging cross-domain fundus imaging datasets demonstrate that Grad-CL outperforms state-of-the-art unsupervised and source-free domain adaptation methods, achieving superior segmentation accuracy and improved boundary delineation. Project and code are available at <https://visdomlab.github.io/GCL/>.

Introduction

Deep convolutional neural networks have achieved remarkable success in segmenting fundus images for glaucoma diagnosis by accurately delineating the optic cup (OC) and optic disc (OD). However, these networks often experience significant performance drop when deployed on new target datasets due to cross-domain discrepancies arising from variations in acquisition protocols, scanner models, and clinical environments. Conventional unsupervised domain adaptation (UDA) methods address these discrepancies by aligning source and target data distributions using both labeled source data and unlabeled target data. In many real-world scenarios, however, the source data may be inaccessible because of copyright restrictions, confidentiality concerns, or computational limitations [1]. This challenge is particularly acute in fundus imaging, where data from different clinical sites exhibit distinct

characteristics. Source-Free Domain Adaptation (SFDA) has emerged as a promising alternative by leveraging a pre-trained source model f^s (trained on $D^s = (X^s, Y^s)$) alongside unlabeled target images. This approach overcomes data privacy and proprietary constraints by eliminating the need for source data during adaptation. Traditional UDA methods rely on explicit alignment of feature distributions—either via specific distance metrics [15] or through adversarial training to learn domain-invariant representations—but these strategies cannot be directly applied in the SFDA setting.

In SFDA, model fine-tuning is commonly achieved through self-supervised training that exploits pseudolabeling, entropy minimization, and contrastive learning. Pseudolabeling generates labels from the pre-trained source model to iteratively refine the model on the target domain. Several approaches, such as SHOT [18], Denoised Pseudolabeling (DPL) [6], and SCNNH [27], rely on computing class prototypes from target features (using techniques like weighted K-means clustering or centroid estimation) to guide pseudolabel assignment. However, these methods often suffer from noisy pseudolabels due to domain shifts and imperfect clustering. DPL is the first work which extended the SFDA model fine-tuning approach for the fundus image segmentation into two classes: optic cup and disc. The class-wise prototypes in DPL are calculated using combined features of the OC and OD for the pseudo label refinement. We hypothesize that instead of using the integrated features from the pre-trained source model, the class-specific features of the OC and OD can be more intuitive for refinement.

Complementary to pseudolabeling, contrastive learning has gained prominence in SFDA by enforcing discriminative feature learning. In the SFDA setting, standard contrastive InfoNCE loss [21] can not be applied due to the absence of target labels. Therefore, SFDA approaches generate positive and negative pairs in a different manner. In the absence of target labels, SFDA approaches generate positive and negative pairs using strategies such as historical source hypotheses or neighborhood information [6]. The historical source hypothesis is the standard approach to handle contrastive SFDA. It contrasts the learned target embeddings of the currently adapted and historical models. HCID [20] involves the usage of memory banks for storage of outputs of historical models. UC-SFDA [6] incorporates neighbourhood-guided evidence-based contrastive loss using Dempster-Shafer theory. DaC [34] learns the global class clustering and local structures by dividing the target into source-like and target-specific samples under adaptive contrastive loss.

Our method (Grad-CL) includes the advantages of both pseudolabeling and contrastive learning for the fundus image segmentation into OC and OD. The inclusion of pseudo-labeling encourages discerning class-wise global assignment, whereas contrastive learning promotes inter-class separability and intra-class compactness at the local structural level. The standard thresholding technique for pseudo-labeling yields noisy labels, followed by the refining step. The uncertainty quantification and class-level prototyping are the important steps for pseudo label refinement. However, in previous works, class-level prototyping leveraged combined features obtained from the class-wise centroid estimation. Grad-CL utilizes Grad-CAM [24] to identify the features that have more impact on identifying OC and OD regions. We calculate the gradients of the segmentation regions with respect to the final convolutional feature layer of the pre-trained source model to obtain the heatmap of the optic cup and disc. Gradient-derived highlighted features of the OC and OD supply richer detail, enabling more precise centroid estimates and consequently superior pseudolabel refinement.

Further, we propose to utilize gradient-derived features of the optic cup and disc as positive and negative pairs for cosine similarity-based contrastive loss. The intuitive idea is to obtain the optic cup and disc features responsible for the final segmentation output and dis-align

them. The dissimilarity between the optic cup and disc features helps in reducing cross-domain discrepancy. The gradient-derived cup and disc features, in collaboration with the combined features from an output of a pre-trained source model, increase the distance between disc and cup in feature space due to contrastive loss, thereby improving the adaptation performance.

2 Related Work

2.1 Unsupervised Domain Adaptation

UDA transmits the information embedded from the labeled source to the unseen, heterogeneous, unlabeled target domain. It mitigates the problem of performance drop due to cross-domain discrepancy and tedious pixel-level annotations. The main categorization of the UDA methods is based on [19]: (a) alignment of the source and target distributions on the basis of specific metrics such as maximum mean discrepancy (MMD) (b) obtaining the domain-invariant features through the adversarial learning (c) image-to-image translation (d) self-training.

In the case of fundus imaging, BEAL [62], pOSAL [63], [8] are state-of-the-art adversarial methods for OC cup and disc segmentation. BEAL [62] and AdvEnt [60] are based on the concept of entropy minimization in the adversarial adaptation network. The source images have low entropy maps, whereas the target produces high entropy maps. The idea is to enforce low entropy on the target with well-designed entropy loss or through indirect minimization with adversarial loss. BEAL utilizes boundary predictions and entropy maps for the alignment of the source and target in an adversarial manner. poSAL [63] is another patch-based adversarial learning method with morphology-aware segmentation loss for generating mask smoothness priors. There are hybrid methods which combine feature alignment, adversarial learning, and image synthesis. For example, the ISFA method combines feature alignment and image synthesis into a single framework for optic cup and disc segmentation [14]. As part of image synthesis from intermediate latent space, the GAN generates the target-like query images. The feature consistency among source, target, and target-like queries is imposed by the content and style feature alignment module. At the final stage, output-level feature alignment generates domain-invariant features adversarially.

2.2 Source Free Domain Adaptation

Pseudolabeling and contrastive learning are widely incorporated in model-finetuning based SFDA methods. The self-training by pseudo labeling implies retraining the network with pseudolabels obtained from a pre-trained source model with the target as the input. The adaptation performance depends on the quality of pseudolabels. There are different self-training based pseudo labeling methods which integrate uncertainty, confidence estimates, and evidential deep learning (EDL) to diminish the effect of poor-quality pseudo labels [8, 12, 23]. Pseudolabel refinement is done through uncertainty quantification through Monte-Carlo drop-out, Laplace approximation, deep ensembles, etc.

Denoised pseudolabeling (DPL) [8], context-aware pseudolabel refinement (CPR) [10], and PLPB [12] are important SFDA techniques catering to the pseudolabel refinement in fundus imaging. DPL generates the pseudo labels by standard thresholding, followed by pseudo label refinement with pixel-level denoising (uncertainty estimation) and class-level denois-

ing (prototype estimation). CPR further extended DPL with the context relations refinement along with pixel-level and class-level denoising. The PLPB method of fundus segmentation introduces additional pseudo boundary loss in addition to the pseudo label loss. The Class-Balanced Mean Teacher (CBMT) [24] framework also addresses the problem of noisy pseudolabels and class imbalance with calibration loss and strong-weak augmented mean teacher model. The aleatoric uncertainty based loss and energy based loss framework refines the pseudo-labels in semi-supervised segmentation setup [28].

It has been observed that the inclusion of contrastive learning in self-training-based pseudolabeling network further improves performance. The local pixel-wise contrastive loss using pseudo labels yields good performance for the self-training-based semi-supervised segmentation [9]. The robust image-classification SFDA network (PLPB) is designed using non-robust pseudo labels and pixel-wise contrastive loss for both clean and adversarial samples [10].

3 Proposed Method

Grad-CL setting uses a pre-trained source model $f^s : X^s \rightarrow Y^s$, trained on the labelled source domain $D^s = (X^s, Y^s)$. The labelled source data is not available during the adaptation stage. The goal of fundus imaging SFDA is to adapt the model f^s with unlabeled target data $\{x_i^t\}_{i=1}^{N_t}$, from the target domain D^t where $x_i^t \in \mathbb{R}^{H \times W \times 3}$ and $y_i^t \in \{0, 1\}^{H \times W \times C}$. In this fundus image segmentation problem, the value of C is two as there are two classes: OC and OD. The output adapted model $f^{s \rightarrow t}$ performs well on the target domain. The fundus image segmentation is a binary label segmentation problem into optic cup and disc regions. Grad-CL integrates two key components to achieve this:

- **Gradient-guided pseudolabel refinement:** Enhances pseudolabel quality using gradient-based feature extraction and prototype estimation.
- **Contrastive feature disalignment:** Encourages inter-class separation between OC and OD regions by minimizing cosine similarity between class-specific gradient-derived features.

The following sections describe each component in detail.

3.1 Gradient-guided pseudolabel refinement

Since target data is unlabeled, we generate initial pseudolabels using the pre-trained source model. Given a target image, the model outputs per-pixel probability maps p_v . We convert these probabilities into binary pseudolabels using a confidence threshold γ :

$$\hat{y}_v^t = \mathbb{1}[p_v \geq \gamma], \quad (1)$$

where $\mathbb{1}(\cdot)$ is the indicator function. Since raw pseudolabels are often noisy due to domain shifts, we refine them using:

(1) Uncertainty-Based Filtering: To filter out unreliable pseudolabels, we estimate pixel-wise uncertainty (u_v) via Monte Carlo dropout by performing K stochastic forward passes. Given probability predictions $\{p_v^{(k)}\}_{k=1}^K$, the uncertainty is computed as:

$$u_v = \sqrt{\frac{1}{K} \sum_{k=1}^K \left(p_v^{(k)} - \bar{p}_v \right)^2}, \quad (2)$$

where \bar{p}_v is the mean probability at pixel v . A binary mask is defined to filter out uncertain predictions:

$$m_v^u = \mathbb{1}[u_v < \eta], \quad (3)$$

where η is the uncertainty threshold.

(2) Gradient-Guided Prototype: To further improve pseudolabel reliability, we extract class-specific gradient-derived features that highlight discriminative structures for optic cup and disc segmentation. Let A^k be the k -th feature map, and y^{cup}, y^{disc} be the logits for the OC and OD, respectively. The gradient-based attention weights are computed by global average pooling over height (h) and width (w) as:

$$\alpha_k^{cup} = \frac{1}{WH} \sum_w \sum_h \frac{\partial y^{cup}}{\partial A_{wh}^k}, \quad \alpha_k^{disc} = \frac{1}{WH} \sum_w \sum_h \frac{\partial y^{disc}}{\partial A_{wh}^k}. \quad (4)$$

The weights α_k^{cup} and α_k^{disc} denote a partial linearization of the source model downstream from k features map A^k , indicating the important pixels in feature maps corresponding to the OC and OD. The gradient based coarse heatmap of OC e_{GC}^{cup} and OD e_{GC}^{disc} highlighting pixels of interest is given by

$$e_{GC}^{cup} = \text{ReLU}\left(\sum_k \alpha_k^{cup} A^k\right), \quad e_{GC}^{disc} = \text{ReLU}\left(\sum_k \alpha_k^{disc} A^k\right). \quad (5)$$

The class-wise prototype calculation involves a binary object mask, binary background mask and combined features multiplied by gradient-specific features. The binary object mask $b^{ob} = \mathbb{1}[\hat{y} = 1] \mathbb{1}[u < \eta]$, binary background mask $b^{bg} = \mathbb{1}[\hat{y} = 0] \mathbb{1}[u < \eta]$, and the modified features are used for the prototype calculation. The modified features are obtained by the multiplication of gradient-derived features e_{GCv} with the combined features e_v , i.e., $e_{GCv} \cdot e_v$. The e_{GCv} denotes the gradient-derived features at pixel v . To refine prototypes, we first extract feature representations e_v from the model's penultimate layer, then augment these features with their corresponding gradient-derived activations:

$$e'_v = e_v \cdot e_{GCv}, \quad (6)$$

where e'_v denotes the enhanced feature representation incorporating gradient-based saliency.

Using the reliable pixels (filtered by uncertainty threshold η), we compute class prototypes:

$$z^{ob} = \frac{\sum_v e'_v b_v^{ob} p_v}{\sum_v b_v^{ob} p_v}, \quad z^{bg} = \frac{\sum_v e'_v b_v^{bg} (1 - p_v)}{\sum_v b_v^{bg} (1 - p_v)}. \quad (7)$$

The relative feature distance of object and background (d_v^{ob}, d_v^{bg}) is also calculated between the modified features and the class prototypes given by

$$d_v^{ob} = \|e_v \cdot e_{GCv} - z^{ob}\|_2, d_v^{bg} = \|e_v \cdot e_{GCv} - z^{bg}\|_2 \quad (8)$$

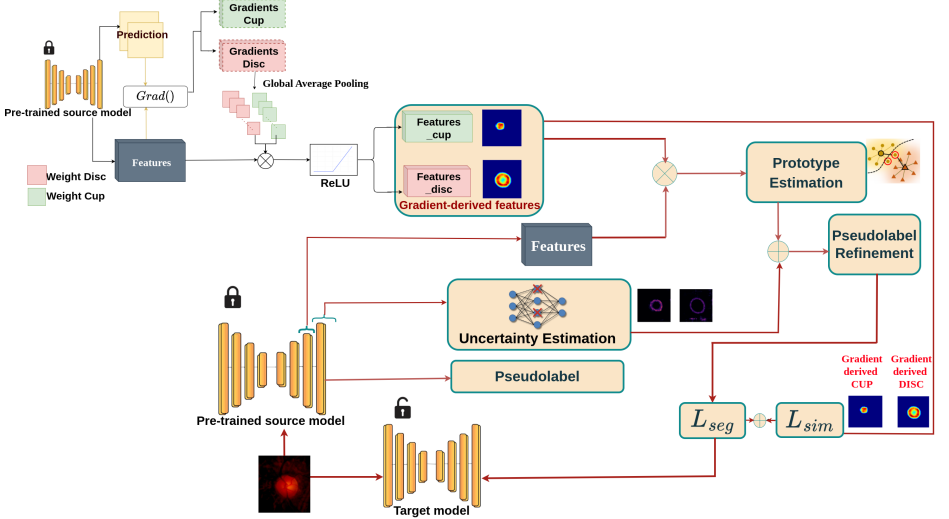


Figure 1: Overview of the proposed Grad-CL technique. The provided target image is fed into a pre-trained source model in order to generate pseudolabels through the process of thresholding. Target domain adaptation consists of two subsequent processes. a) *Pseudolabel Refinement*: This process involves estimating uncertainty and deriving prototypes using gradients. b) *Contrastive Loss Module*: This module is used to calculate the contrastive loss. The similarity measure \mathcal{L}_{sim} is computed using modified gradient-derived features of the cup and disc.

The pseudolabel is considered noisy if the modified feature vector derived using gradient function ($\{e_v \cdot e_{GC_v}\}$) is further away from the object prototype z^{ob} rather than the background prototype z^{bg} . This distance wise denoising is merged with uncertainty based denoising to obtain the modified mask as:

$$m_v = \mathbb{1}[u_v < \eta] [\hat{y}_v^t = 1] \left[d_v^{ob} < d_v^{bg} \right] + \mathbb{1}[u_v < \eta] [\hat{y}_v^t = 0] \left[d_v^{ob} > d_v^{bg} \right] \quad (9)$$

The pseudolabel $\hat{y}_v^t = 1$ represents the object region, whereas $\hat{y}_v^t = 0$ represents background region. So, this binary mask m_v can be used with standard-cross entropy for the adaptation. It leverages both uncertainty information and gradient-derived prototype estimation information. The final segmentation loss is computed as:

$$\mathcal{L}_{seg} = \sum_v m_v \cdot \mathcal{L}_{ce,v} \quad (10)$$

where $\mathcal{L}_{ce,v}$ is the per-pixel cross-entropy loss with pseudolabels.

3.2 Contrastive Feature Disalignment

Despite refined pseudolabels, feature overlaps between the OC and OD can still lead to misclassification. To address this, we introduce contrastive learning to explicitly enforce feature disalignment. The gradient modified features highlight the key features of the optic cup and disc. We propose to utilize gradient highlighted feature, i.e., e_{GC}^{cup} and e_{GC}^{disc} , along with

the combined features obtained from the network. The disalignment of the key features of the cup the disc by cosine similarity loss supports adaptation by creating contrast between class-specific features. Although, the combined features e_v have attributes responsible for segmentation of both cup and disc. We can modify this combined features e_v with the addition of gradient based feature map $e_{GCv}^{cup}, e_{GCv}^{disc}$ pertaining to key regions which are actually responsible for cup and disc output. As there are regions of misinterpretation where the cup is identified as a disc and vice-versa. Therefore, the disalignment of the embeddings obtained from $(e_v + e_{GCv}^{cup})$ and $(e_v + e_{GCv}^{disc})$ will reduce the similarity between cup and disc features with every epoch.

We construct gradient-informed class-specific representations:

$$\tilde{e}_v^{cup} = e_v + e_{GCv}^{cup}, \quad \tilde{e}_v^{disc} = e_v + e_{GCv}^{disc}. \quad (11)$$

We then compute the cosine similarity loss:

$$\mathcal{L}_{sim} = \frac{\tilde{e}_v^{cup} \cdot \tilde{e}_v^{disc}}{\max(\|\tilde{e}_v^{cup}\|_2 \|\tilde{e}_v^{disc}\|_2, \epsilon)}, \quad (12)$$

where ϵ prevents division by zero.

The overall training loss is a combination of segmentation and contrastive losses:

$$\mathcal{L}_{total} = \mathcal{L}_{seg} + \lambda \mathcal{L}_{sim}, \quad (13)$$

where λ balances segmentation and contrastive objectives.

Grad-CL effectively refines noisy pseudolabels using **gradient-enhanced feature extraction** while **contrastive learning** disaligns optic cup and disc representations. This results in improved segmentation performance under source-free adaptation. Figure 1 depicts block diagram of Grad-CL method.

Table 1 summarizes the performance of Grad-CL compared to several state-of-the-art methods, illustrating the effectiveness of our refined pseudolabeling and contrastive learning strategy. The detailed steps are given in Algorithm 1.

Methods	S-F	Optic Disc		Optic Cup		Optic Disc		Optic Cup	
		Dice% \uparrow	ASD \downarrow	Dice% \uparrow	ASD \downarrow	Dice% \uparrow	ASD \downarrow	Dice% \uparrow	ASD \downarrow
RIM-ONE-r3					Drishti-GS				
W/o adaptation		83.18	24.15	74.51	14.44	93.84	9.05	83.36	11.39
Oracle [65]		96.80	-	85.60	-	96.40	-	90.10	-
BEAL [65]		89.80	-	81.00	-	96.10	-	86.20	-
OCDA [66]	No	86.47	16.76	76.74	10.94	-	-	-	-
AdvEnt [66]	No	89.73	9.84	77.99	7.57	96.16	4.36	82.75	11.36
SRDA [66]	No	89.37	9.91	77.61	10.15	96.22	4.88	80.67	13.12
DAE [66]	No	89.08	11.63	79.01	10.31	94.04	8.79	83.11	11.56
TT-SFUDA [66]	Yes	85.00	17.05	76.62	10.31	95.22	6.00	80.67	13.00
TENT [66]	Yes	82.92	23.63	72.95	14.00	94.06	7.56	80.12	13.52
PLPB [66]	Yes	92.89	6.52	77.94	10.07	96.51	4.01	83.56	11.11
DPL [66]	Yes	90.13	9.43	79.78	9.01	96.39	4.08	83.53	11.39
Proposed (Grad-CL)	Yes	94.99	5.02	80.51	9.50	96.58	4.09	84.67	10.28

Table 1: Quantitative Performance of Various State-of-the-Art UDA and SFDA Methods on Target Datasets: RIM-ONE-r3 [10] and Drishti-GS [10]. Refuge [10] is taken as the Source Dataset to train the source model for adaptation.

Algorithm 1: Source-Free Domain adaptation of fundus images using pseudolabel refinement and contrastive loss with gradient activations

Input: Pre-trained source model $f^s(x^s \rightarrow y^s)$,
 Penultimate layer feature maps A ,
 Prediction probability p_v ,
 Unlabeled target data $\{x_i^t\}_{i=1}^{N_t} \in D^t$

Output: Adapted segmentation model $f^{s \rightarrow t}(\hat{\theta}_c)$

- 1 **for** each mini-batch of unlabeled samples $X_i^t \in D^t$ **do**
- 2 **Self-training;**
- 3 $\mathcal{L}_{ce,v} \leftarrow CE(\hat{y}_v^t, p_v)$, where \hat{y}_v^t are pseudolabels;
- 4 **Gradient-derived cup and disc features;**
- 5 Output logits $y, y^{cup} = y[:, 0 : 1, :, :], y^{disc} = y[:, 1, :, :]$
- 6 $\alpha_k^{cup} = \text{GAP}(\text{grad}(y^{cup}, A^k))$;
- 7 $\alpha_k^{disc} = \text{GAP}(\text{grad}(y^{disc}, A^k))$;
- 8 $e_{GC}^{cup} = \text{ReLU}(\sum_k \alpha_k^{cup} A^k)$;
- 9 $e_{GC}^{disc} = \text{ReLU}(\sum_k \alpha_k^{disc} A^k)$;
- 10 **Pseudolabel refinement;**
- 11 Define uncertainty threshold η ;
- 12 Compute prototypes using e_{GC}^{cup} and e_{GC}^{disc} ;
- 13 Calculate distance vectors $d_v^{ob} = \|e_v \cdot e_{GCv} - z^{ob}\|_2$;
- 14 $d_v^{bg} = \|e_v \cdot e_{GCv} - z^{bg}\|_2$;
- 15 **Modified initial CE loss;**
- 16 Define modified mask m_v using eq. 10;
- 17 $\mathcal{L}_{seg} = \sum_v m_v \cdot \mathcal{L}_{ce,v}$;
- 18 **Contrastive loss;**
- 19 $\mathcal{L}_{sim} = \text{Cosine Similarity between } \{(e_v + e_{GCv}^{cup}, e_v + e_{GCv}^{disc})\}$;
- 20 **Total loss;**
- 21 $\mathcal{L}_{total} = \mathcal{L}_{seg} + \mathcal{L}_{sim}$;
- 22 **end**
- 23 **Output:** Trained adapted segmentation parameters $\hat{\theta}_c$;

4 Experiments

Datasets: We follow the setup in [6, 32] by using the open-source REFUGE Challenge [32] as the source dataset and Drishti-GS [25] and RIM-ONE-r3 [9] as target datasets. The source comprises 400 annotated images (combining train and test splits), while the targets use 99/60 and 50/51 train/test splits for Drishti-GS and RIM-ONE-r3, respectively. Each image is preprocessed by extracting a 512×512 region-of-interest that captures the cup and disc. We evaluate segmentation performance using the Dice Coefficient and Average Surface Distance (ASD).

Implementation Details: The pre-trained source model f_s generates pseudolabels on target images using a threshold of 0.75 [6, 32]. Uncertainty-based refinement employs Monte-Carlo dropout (rate 0.5) with an uncertainty threshold of 0.05 over 10 stochastic passes. For prototype estimation, gradient-highlighted features are used. Our segmentation network is DeepLabv3+ [4] with a MobileNetv2 backbone, trained with the Adam optimizer (momentum 0.9–0.99, learning rate 2×10^{-3}). During adaptation, weak augmentations (random erasing, contrast modification, and Gaussian noise) are applied to slightly perturb inputs and encourage divergence from the pseudolabels. The target model $f^{s \rightarrow t}$ is trained using \mathcal{L}_{total} for 20 epochs with a batch size of 8 on PyTorch 1.12.1 and an NVIDIA A100 GPU.

Comparative Analysis: In this comparative analysis, we perform quantitative evaluations

Drishti-GS					RIM-ONE-r3			
	Cup	Disc	Cup	Disc	Cup	Disc	Cup	Disc
Metric	Dice Score		ASD Score		Dice Score		ASD Score	
KL divergence	84.53	96.58	10.38	4.05	80.46	95.07	9.58	4.98
JS divergence	84.46	96.53	10.45	4.15	79.91	95.24	9.89	4.78
MMD	83.36	96.54	11.23	4.13	77.44	94.29	10.49	6.11
Euclidean	80.11	91.51	13.54	11.93	63.87	72.63	13.62	53.63

Table 2: ASD and Dice Coefficient on Drishti-GS and RIM-ONE-r3 using different distance/divergence metrics between gradient-based feature maps of the cup and disc.

using several baselines and state-of-the-art methods—namely, a without adaptation baseline (lower bound), a supervised adaptation baseline (Oracle) in the target domain, unsupervised domain adaptation (UDA) methods (e.g., BEAL [52], AdvEnt [50], OCDA [20], SRDA [9], DAE [33]) and source-free domain adaptation (SFDA) methods (e.g., TT-SFUDA [49], TENT [51], DPL [6], PLPB [37]) as reported in Table 1; (i) among the UDA methods, BEAL stands out as a benchmark that employs adversarial learning based on boundary predictions and entropy maps between the source and target, making it the best reported UDA method for fundus image segmentation, while AdvEnt is built on entropy minimization, OCDA utilizes a curriculum domain adaptation strategy with memory modules to enhance generalization in open and compound domains, SRDA leverages entropy minimization with a source-trained task prior, and DAE incorporates an implicit prior through denoising autoencoders; (ii) in contrast, most SFDA methods for fundus imaging rely on self-training with pseudo-labeling—with DPL serving as a benchmark for pseudo-label refinement via uncertainty and prototype estimation and PLPB combining entropy minimization with a pseudo-boundary loss for open domain adaptation—yet these approaches tend to fuse the features of the optic cup and disc for prototype estimation, occasionally resulting in misidentification between the two regions; our proposed method, Grad-CL, addresses this limitation by explicitly disaligning cup and disc features through a contrastive loss that utilizes gradient-derived features, thereby enhancing prototype estimation and ultimately outperforming the aforementioned SFDA methods. Most SFDA methods in fundus imaging rely on self-training with pseudolabeling. DPL refines pseudolabels using uncertainty and prototype estimation, while PLPB incorporates entropy minimization with a pseudo-boundary loss. In contrast, Grad-CL not only refines pseudolabels but also disaligns cup and disc features through a contrastive loss, thereby reducing misclassification between these regions.

Figures 2 and 3 display segmentation overlays for RIM-ONE-r3 and Drishti-GS, respectively, comparing the results of Grad-CL with DPL, CPR, and BEAL.

Ablation Study: Table 2 evaluates several metrics applied to gradient-based feature maps of the optic cup and disc on the Drishti-GS and RIM-ONE-r3 datasets by comparing divergence metrics (KL and JS divergences) with distance metrics (MMD and Euclidean) using the Dice Coefficient and Average Surface Distance (ASD) as evaluation measures; (i) the divergence metrics yielded high Dice scores (e.g., for Drishti-GS, cup: 84.53 with KL and 84.46 with JS, disc: 96.58 with KL and 96.53 with JS; similar trends were observed on RIM-ONE-r3) along with low ASD values (approximately 10.38–10.45 for the cup and 4.05–4.15 for the disc), and (ii) in contrast, the distance metrics, particularly Euclidean distance, resulted in significantly lower Dice scores and higher ASD values (e.g., on Drishti-GS, cup: 80.11 and disc: 91.51 with Euclidean, accompanied by ASD values up to 13.54 and 11.93, respectively), indicating that enforcing divergence between cup and disc features is more effective than minimizing Euclidean distances in high-dimensional feature spaces; overall, these find-

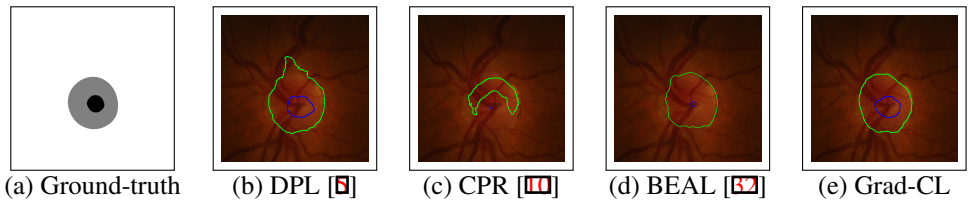


Figure 2: Overlaying the final segmentation on an image from the RIM-ONE-r3 dataset. The blue outline denotes the cup and the green outline denotes the disc. Competing methods show visibly stretched or contracted regions relative to **Grad-CL**.

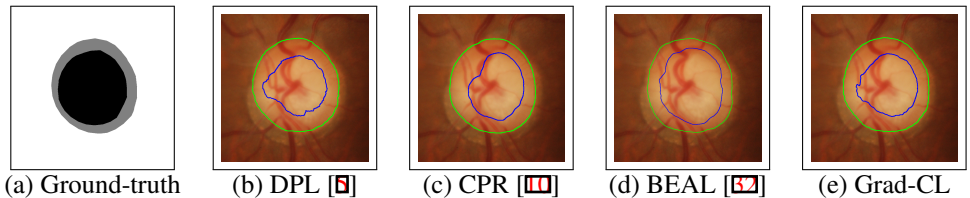


Figure 3: Final segmentation overlay on a Drishti-GS image. The blue outline marks the optic cup; the green outline marks the optic disc. Alternative methods show deformation relative to the proposed **Grad-CL**.

ings demonstrate that explicitly modeling the divergence between feature distributions not only enhances segmentation performance but can also slightly surpass the performance of traditional cosine similarity losses, especially for optic disc segmentation.

5 Conclusion

Grad-CL, a novel SFDA approach for fundus imaging leverages gradient-derived features for enhanced pseudolabel refinement and a contrastive loss to disalign cup and disc features. The inclusion of feature gradient information in prototype estimation and cosine-similarity contrastive loss improves the results. Our method demonstrates performance that is on par with or superior to state-of-the-art source-dependent and source-free approaches. An ablation study validates that enforcing divergence between the gradient-based activations of the cup and disc is crucial for improved segmentation. In future work, we plan to explore advanced gradient-based feature extraction techniques (e.g., Score-CAM, Grad-CAM++, Relevance-CAM) and incorporate source distribution information to further address pronounced domain shifts.

Acknowledgments Rini acknowledges the financial support provided by the Department of Science and Technology, Government of India, through the DST WISE Post-Doctoral Fellowship Program (Reference No. DST/WISE-PDF/ET-33/2023), which facilitated the successful completion of this work. Rajeev acknowledges the support received from the TCS PhD fellowship (Cycle 18).

References

- [1] Peshal Agarwal, Danda Pani Paudel, Jan-Nico Zaech, and Luc Van Gool. Unsupervised robust domain adaptation without source data. In *Proceedings of the IEEE/CVF Winter Conference on Applications of Computer Vision*, pages 2009–2018, 2022.
- [2] Mathilde Bateson, Hoel Kervadec, Jose Dolz, Hervé Lombaert, and Ismail Ben Ayed. Source-relaxed domain adaptation for image segmentation. In Anne L. Martel, Purang Abolmaesumi, Danail Stoyanov, Diana Mateus, Maria A. Zuluaga, S. Kevin Zhou, Daniel Racoceanu, and Leo Joskowicz, editors, *Medical Image Computing and Computer Assisted Intervention – MICCAI 2020*, pages 490–499, Cham, 2020. Springer International Publishing. ISBN 978-3-030-59710-8.
- [3] Charles Blundell, Julien Cornebise, Koray Kavukcuoglu, and Daan Wierstra. Weight uncertainty in neural network. In *International conference on machine learning*, pages 1613–1622. PMLR, 2015.
- [4] Krishna Chaitanya, Ertunc Erdil, Neerav Karani, and Ender Konukoglu. Local contrastive loss with pseudo-label based self-training for semi-supervised medical image segmentation. *Medical Image Analysis*, 87:102792, 2023.
- [5] Cheng Chen, Quande Liu, Yueming Jin, Qi Dou, and Pheng-Ann Heng. Source-free domain adaptive fundus image segmentation with denoised pseudo-labeling. In *Medical Image Computing and Computer Assisted Intervention–MICCAI 2021: 24th International Conference, Strasbourg, France, September 27–October 1, 2021, Proceedings, Part V 24*, pages 225–235. Springer, 2021.
- [6] Dong Chen, Hongqing Zhu, and Suyi Yang. Uc-sfda: Source-free domain adaptation via uncertainty prediction and evidence-based contrastive learning. *Knowledge-Based Systems*, 275:110728, 2023. ISSN 0950-7051. doi: <https://doi.org/10.1016/j.knosys.2023.110728>. URL <https://www.sciencedirect.com/science/article/pii/S0950705123004781>.
- [7] Liang-Chieh Chen, Yukun Zhu, George Papandreou, Florian Schroff, and Hartwig Adam. Encoder-decoder with atrous separable convolution for semantic image segmentation. In *Proceedings of the European conference on computer vision (ECCV)*, pages 801–818, 2018.
- [8] Wei Feng, Lin Wang, Lie Ju, Xin Zhao, Xin Wang, Xiaoyu Shi, and Zongyuan Ge. Unsupervised domain adaptive fundus image segmentation with category-level regularization. In *International Conference on Medical Image Computing and Computer-Assisted Intervention*, pages 497–506. Springer, 2022.
- [9] Francisco Fumero, Silvia Alayón, José L Sanchez, Jose Sigut, and M Gonzalez-Hernandez. Rim-one: An open retinal image database for optic nerve evaluation. In *2011 24th international symposium on computer-based medical systems (CBMS)*, pages 1–6. IEEE, 2011.
- [10] Zheang Huai, Xinpeng Ding, Yi Li, and Xiaomeng Li. Context-aware pseudo-label refinement for source-free domain adaptive fundus image segmentation. In *International Conference on Medical Image Computing and Computer-Assisted Intervention*, pages 618–628. Springer, 2023.

- [11] Jiaxing Huang, Dayan Guan, Aoran Xiao, and Shijian Lu. Model adaptation: Historical contrastive learning for unsupervised domain adaptation without source data. *Advances in Neural Information Processing Systems*, 34:3635–3649, 2021.
- [12] Alex Kendall and Yarin Gal. What uncertainties do we need in bayesian deep learning for computer vision? *Advances in neural information processing systems*, 30, 2017.
- [13] Dong-Hyun Lee et al. Pseudo-label: The simple and efficient semi-supervised learning method for deep neural networks. In *Workshop on challenges in representation learning, ICML*, volume 3, page 896. Atlanta, 2013.
- [14] Haijun Lei, Weixin Liu, Hai Xie, Benjian Zhao, Guanghui Yue, and Baiying Lei. Unsupervised domain adaptation based image synthesis and feature alignment for joint optic disc and cup segmentation. *IEEE Journal of Biomedical and Health Informatics*, 26(1):90–102, 2021.
- [15] Jingjing Li, Erpeng Chen, Zhengming Ding, Lei Zhu, Ke Lu, and Heng Tao Shen. Maximum density divergence for domain adaptation. *IEEE Transactions on Pattern Analysis and Machine Intelligence*, 43(11):3918–3930, 2021. doi: 10.1109/TPAMI.2020.2991050.
- [16] Jingjing Li, Zhiqi Yu, Zhekai Du, Lei Zhu, and Heng Tao Shen. A comprehensive survey on source-free domain adaptation. *IEEE Transactions on Pattern Analysis and Machine Intelligence*, 46(8):5743–5762, 2024. doi: 10.1109/TPAMI.2024.3370978.
- [17] Lingrui Li, Yanfeng Zhou, and Ge Yang. Robust source-free domain adaptation for fundus image segmentation. In *2024 IEEE/CVF Winter Conference on Applications of Computer Vision (WACV)*, pages 7825–7834, 2024. doi: 10.1109/WACV57701.2024.00766.
- [18] Jian Liang, Dapeng Hu, and Jiashi Feng. Do we really need to access the source data? source hypothesis transfer for unsupervised domain adaptation. In *International conference on machine learning*, pages 6028–6039. PMLR, 2020.
- [19] Xiaofeng Liu, Chaehwa Yoo, Fangxu Xing, Hyejin Oh, Georges El Fakhri, Je-Won Kang, Jonghye Woo, et al. Deep unsupervised domain adaptation: A review of recent advances and perspectives. *APSIPA Transactions on Signal and Information Processing*, 11(1), 2022.
- [20] Ziwei Liu, Zhongqi Miao, Xingang Pan, Xiaohang Zhan, Dahua Lin, Stella X Yu, and Boqing Gong. Open compound domain adaptation. In *Proceedings of the IEEE/CVF Conference on Computer Vision and Pattern Recognition*, pages 12406–12415, 2020.
- [21] Aaron van den Oord, Yazhe Li, and Oriol Vinyals. Representation learning with contrastive predictive coding. *arXiv preprint arXiv:1807.03748*, 2018.
- [22] José Ignacio Orlando, Huazhu Fu, João Barbosa Breda, Karel van Keer, Deepti R. Bathula, Andrés Diaz-Pinto, Ruogu Fang, Pheng-Ann Heng, Jeyoung Kim, JoonHo Lee, Joonseok Lee, Xiaoxiao Li, Peng Liu, Shuai Lu, Balamurali Murugesan, Valery Naranjo, Sai Samarth R. Phaye, Sharath M. Shankaranarayana, Apoorva Sikka, Jaemin Son, Anton van den Hengel, Shujun Wang, Junyan Wu, Zifeng Wu, Guanghui

- Xu, Yongli Xu, Pengshuai Yin, Fei Li, Xiulan Zhang, Yanwu Xu, and Hrvoje Bogunović. Refuge challenge: A unified framework for evaluating automated methods for glaucoma assessment from fundus photographs. *Medical Image Analysis*, 59:101570, 2020. ISSN 1361-8415. doi: <https://doi.org/10.1016/j.media.2019.101570>. URL <https://www.sciencedirect.com/science/article/pii/S1361841519301100>.
- [23] Shivangi Rai, Rini Smita Thakur, Kunal Jangid, and Vinod K Kurmi. Label calibration in source free domain adaptation. In *2025 IEEE/CVF Winter Conference on Applications of Computer Vision (WACV)*, pages 6446–6455, 2025. doi: 10.1109/WACV61041.2025.00628.
- [24] Ramprasaath R Selvaraju, Michael Cogswell, Abhishek Das, Ramakrishna Vedantam, Devi Parikh, and Dhruv Batra. Grad-cam: Visual explanations from deep networks via gradient-based localization. In *Proceedings of the IEEE international conference on computer vision*, pages 618–626, 2017.
- [25] Jayanthi Sivaswamy, S Krishnadas, Arunava Chakravarty, G Joshi, A Syed Tabish, et al. A comprehensive retinal image dataset for the assessment of glaucoma from the optic nerve head analysis. *JSM Biomedical Imaging Data Papers*, 2(1):1004, 2015.
- [26] Longxiang Tang, Kai Li, Chunming He, Yulun Zhang, and Xiu Li. Source-free domain adaptive fundus image segmentation with class-balanced mean teacher. In Hayit Greenspan, Anant Madabhushi, Parvin Mousavi, Septimiu Salcudean, James Duncan, Tanveer Syeda-Mahmood, and Russell Taylor, editors, *Medical Image Computing and Computer Assisted Intervention – MICCAI 2023*, pages 684–694, Cham, 2023. Springer Nature Switzerland. ISBN 978-3-031-43907-0.
- [27] Song Tang, Yan Yang, Zhiyuan Ma, Norman Hendrich, Fanyu Zeng, Shuzhi Sam Ge, Changshui Zhang, and Jianwei Zhang. Nearest neighborhood-based deep clustering for source data-absent unsupervised domain adaptation. *arXiv preprint arXiv:2107.12585*, 2021.
- [28] Rini Smita Thakur and Vinod K Kurmi. Uncertainty and energy based loss guided semi-supervised semantic segmentation. In *2025 IEEE/CVF Winter Conference on Applications of Computer Vision (WACV)*, pages 8035–8045, 2025. doi: 10.1109/WACV61041.2025.00780.
- [29] S. Vibashan, V. Jeya Maria Jose Valanarasu, and Vishal M. Patel. Target and task specific source-free domain adaptive image segmentation. In *Proceedings of the Medical Imaging with Deep Learning (MIDL)*, pages 1627–1639, June 2024.
- [30] Tuan-Hung Vu, Himalaya Jain, Maxime Bucher, Matthieu Cord, and Patrick Pérez. Advent: Adversarial entropy minimization for domain adaptation in semantic segmentation. In *Proceedings of the IEEE/CVF conference on computer vision and pattern recognition*, pages 2517–2526, 2019.
- [31] Dequan Wang, Evan Shelhamer, Shaoteng Liu, Bruno Olshausen, and Trevor Darrell. Tent: Fully test-time adaptation by entropy minimization. In *Proceedings of the 9th International Conference on Learning Representations (ICLR)*, 2021. URL <https://openreview.net/forum?id=uXl3bZLkr3c>. Spotlight Paper.

-
- [32] Shujun Wang, Lequan Yu, Kang Li, Xin Yang, Chi-Wing Fu, and Pheng-Ann Heng. Boundary and entropy-driven adversarial learning for fundus image segmentation. In *Medical Image Computing and Computer Assisted Intervention–MICCAI 2019: 22nd International Conference, Shenzhen, China, October 13–17, 2019, Proceedings, Part I* 22, pages 102–110. Springer, 2019.
 - [33] Shujun Wang, Lequan Yu, Xin Yang, Chi-Wing Fu, and Pheng-Ann Heng. Patch-based output space adversarial learning for joint optic disc and cup segmentation. *IEEE transactions on medical imaging*, 38(11):2485–2495, 2019.
 - [34] Ziyi Zhang, Weikai Chen, Hui Cheng, Zhen Li, Siyuan Li, Liang Lin, and Guanbin Li. Divide and contrast: Source-free domain adaptation via adaptive contrastive learning. *Advances in Neural Information Processing Systems*, 35:5137–5149, 2022.